Dimensioning Flat Equivalent Radiators

Amedeo Capozzoli, *Member, IEEE*, Claudio Curcio, *Member, IEEE*, and Angelo Liseno

***Abstract*— We deal with the problem of modeling a radiator/scatterer using an equivalent radiator. The problem amounts at determining shape and size of a radiating surface $\mathscr{D}'$ producing, on a region $\mathscr{D}$, an electromagnetic field close to that generated by the primary radiator/scatterer. For a fixed equivalent radiator's shape, we deal here with the dimensioning issue only. The approach exploits the singular value decomposition (SVD) of the operators relating the radiator/scatterer to the field on $\mathscr{D}$ and the equivalent panel to the field on $\mathscr{D}$. The size of the equivalent radiator is determined by minimizing the error between the primary radiated/scattered field and that radiated using $\mathscr{D}'$. The error is expressed as a Hermitian, positive semidefinite quadratic form: the dimensioning problem thus consists of determining the size of the equivalent radiator maximizing its minimum eigenvalue. The maximization is performed by choosing the size value leading to an error dropping below a prescribed maximum tolerated threshold. We present numerical test cases for a planar radiator with rectangular shape.**

***Index Terms*— Dimensioning, echo generators, quadrature, singular functions, singular value decomposition (SVD), singular value optimization (SVO).**

I. Introduction

THE problem of modeling a source or a scatterer using an equivalent radiator is of interest in a large number of applications.

For example, in antenna synthesis [1], once the specifications on the far-field [2] and/or the near-field [3] regions are settled, determining the size and possibly the shape [4] of a minimum-sized antenna capable to meet the prescriptions becomes of interest. Furthermore, in order to characterize the radiating behavior of antennas from near-field data, a preliminary step is determining the size of effective sources capable to match the near-field measurements [5], [6]. Similarly, in applications of electromagnetic compatibility, the problem of evaluating the far-field emissions produced by a printed circuit board (PCB) arises. Notwithstanding the need of applying coherence theory to the source at hand (partial coherence or total incoherence), also in this case, the determination of the dimensions of an equivalent source capable to match the near-field measurements is necessary [7]. In the framework of the design of complex waveform generators [8], which can be of interest in the recent applications of automotive radar testing [9], one of the hottest problems to be solved is that of determining the dimensions of a radiating panel capable to simulate the radar echo produced by canonical scatterers to test the performance of anticollision radars [10]. Finally, the dimensioning problem is also relevant for computational electromagnetics applications and inverse scattering in order to provide partial representations of the scattered fields to reduce the number of unknowns in describing the scattering process and improving inverse scattering problem solutions [11], [12].

The problem can be formulated as that of determining the shape and dimensions of a radiating surface $\mathscr{D}'$ capable to produce an electromagnetic field $\underline{E}_2$ as close as possible to $\underline{E}_1$, where $\underline{E}_1$ is the field generated by the "primary" radiator/scatterer in a targeted region $\mathscr{D}$ and $\underline{E}_2$ is the field radiated by the "equivalent" source $\mathscr{D}'$ on $\mathscr{D}$ again.

In this sense, the panel $\mathscr{D}'$ is "equivalent" to the primary sources/scatterers.

As weak information, we assume here geometrical information on the sources/scatterers and, in particular, that they are confined to a sphere $\mathscr{S}$ of a certain known radius a_R. The sphere $\mathscr{S}$ can be representative of a true source or an equivalent one arising from a scattering process. Although here the region containing the sources/scatterers is assumed spherical, the method is by no means limited by such an assumption. The knowledge of the sphere radius and of the reciprocal geometry between $\mathscr{S}$ and $\mathscr{D}$ determines the set of fields to be approximated.

The formulation is given in a clear and unique mathematical setting so that the problem involves the determination of effective subspaces and operators linking them. The solution is provided by a classical tool of linear algebra, namely, the singular value decomposition (SVD) of the following:

1) the operator $\mathscr{A}_1$ linking the radiator/scatterer to $\underline{E}_1$;
2) the operator $\mathscr{A}_2$ linking the equivalent radiating panel to $\underline{E}_2$.

The singular functions of such operators associated with the most significant singular values define the linear subspaces to which $\underline{E}_1$ and $\underline{E}_2$ belong. We determine the dimensions of the equivalent radiator to reduce, as much as possible, the error by which $\underline{E}_2$ approximates $\underline{E}_1$, independently of the radiated/scattered field $\underline{E}_1$. We show that the error can be represented as a Hermitian, positive-definite quadratic form and prove that the problem can be tackled as the maximization of its minimum eigenvalue. The maximization is practically performed by choosing the mentioned dimensions leading to an error dropping below a prescribed maximum tolerated threshold.

The SVD is a well-established tool of linear algebra that dates back to the XIX century and that enables a decomposition analysis of linear operators between

Manuscript received 27 May 2021; revised 14 March 2022; accepted 20 March 2022. Date of publication 15 May 2023; date of current version 7 July 2023. *(Corresponding author: Amedeo Capozzoli.)*

The authors are with the Dipartimento di Ingegneria Elettrica e delle Tecnologie dell'Informazione, Universitá di Napoli Federico II, 80125 Naples, Italy (e-mail: a.capozzoli@unina.it).

Color versions of one or more figures in this article are available at https://doi.org/10.1109/TAP.2023.3260919.

Digital Object Identifier 10.1109/TAP.2023.3260919

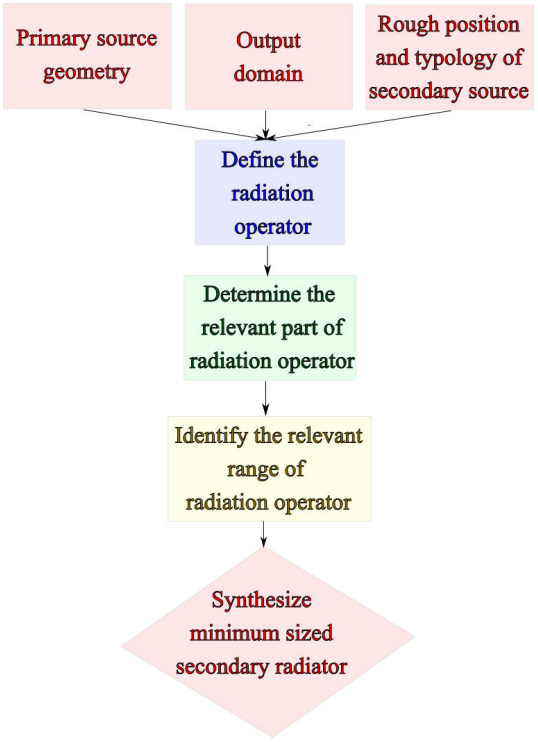

Fig. 1. Flowchart of the approach.

finite-dimensional spaces. It has been extended also to the case of infinite-dimensional spaces by the singular value expansion. SVD enables to enucleate the relevant part of a linear operator when the singular value dynamics is analyzed. In particular, it returns the relevant input and output vector spaces [13], [14], [15], [16], [17], [18], [19], [20], [21]. Furthermore, depending on the adopted scheme, it also enables a regularization of the inversion process.

The purpose of this article is, however, identifying the relevant part of linear operators using SVD. Our full procedure is shown in Fig. 1.

1) Give the following:
   a) the geometry of the primary source;
   b) the output domain $\mathscr{D}$;
   c) a rough position and typology of the secondary source (e.g., surface radiator of rectangular shape).
2) Define the radiation operator $\mathscr{A}_1$.
3) Determine the relevant part of $\mathscr{A}_1$.
4) Identify the relevant range of $\mathscr{A}_1$, namely, the subspace of the fields radiated over $\mathscr{D}$.
5) Synthesize a minimum-sized secondary source so that, once defined $\mathscr{A}_2$, the range of $\mathscr{A}_2$ contains that of $\mathscr{A}_1$; in this way, $\mathscr{A}_2$ is capable to radiate, over $\mathscr{D}$, all the fields that can be radiated by $\mathscr{A}_1$, according to a prescribed tolerance.

We explicitly mention that the approach proposed in this article can also be exploited in the field of plane wave synthesis and, in particular, to determining the dimensions of the radiating panel by which tilted plane waves having tilt angle within a preassigned cone can be accurately radiated in a quiet-zone region [8].

In this article, we consider the particular case of a flat panel of rectangular shape and a flat domain $\mathscr{D}$ parallel to $\mathscr{D}'$ again of rectangular shape and propose an approach for the solution of the dimensioning problem. For the sake of simplicity, a scalar problem is considered. Such assumptions will by no means limit the validity of the approach and will enable to expound all the theoretical aspects of the method.

The solution is new and, to the best of our knowledge, the dealt-with problem has not been yet consistently faced in all its aspects. The first results of this approach have been presented in [22], while the first ideas were published in [23], [24], and [25]. However, the following conditions hold.

1) All the mathematical aspects of the method just sketched in [24] are presented.
2) Full mathematical proofs of the main results, with particular attention to the approximation error expressed as a Hermitian positive-definite quadratic form, are presented.
3) An extensive numerical analysis, with totally new test cases, involving a planar scatterer, an aggregate of small scattering spheres, and a solitary scattering sphere are shown.

The approach dealt with in this article permits to face the problem in its generality, in particular, by enabling to determine the shape and dimensions of the radiating panel by minimizing the maximum approximation error. Here, we focus the attention on the only determination of the size of the equivalent radiator.

We mention that Maisto et al. [26] considered a problem similar to the one dealt with in the present contribution with three main differences: 1) it is 2-D, while ours is 3-D and dismisses any factorization of the spatial variables; 2) the source is a strip instead of a sphere; and 3) the domain of interest is in the far zone, while it is located in the near zone in our manuscript. In [26], the matching between the fields associated with the radiator/scatterer and the panel is performed uniquely based on matching between the dimensions of their respective involved embedding vector spaces. Of course, by this, a representation within a prescribed relative error is not possible. Here, the matching considers the actual properties of the vector spaces embedding the fields of interest and relies on the more complete capability of approximating any field radiated by the source/scatterer with a field radiated by a proper panel, guaranteeing a desired degree of accuracy.

This article is organized as follows. In Section II, the dimensioning problem is presented in its mathematical detail. Section III is devoted to the presentation of the solution approach, while Section IV contains the numerical analysis. Finally, in Section V, the conclusions are gathered and future developments foreseen.

II. Problem

The geometry of the considered problem is shown in Fig. 2. The sphere $\mathscr{S}$ has radius a_R and encloses one or more sources and/or scatterers Σ. The domain of interest $\mathscr{D}$ on which we want to reproduce the field generated by Σ is a rectangular portion of plane of dimensions $2a \times 2b$, set a distance $\overline{d}$ apart from the center of $\mathscr{S}$. On introducing the $Oxyz$, $O'x'y'z'$,

and $O''x''y''z''$ coordinate systems as in Fig. 2, behind $\mathscr{S}$, a radiating panel $\mathscr{D}'$ is positioned at a distance d' apart from the center of the sphere. The radiating panel is once again a rectangular portion of plane, this time of dimensions $2a' \times 2b'$, parallel to $\mathscr{D}$ and located a distance $d = \overline{d} - d'$ apart from it.

We remark that the presence of Σ and of the radiating panel $\mathscr{D}'$ is reciprocally exclusive. The enclosing sphere and the radiating panel are never present simultaneously since the radiating panel has the task to radiate the same field of the objects within $\mathscr{S}$.

In this article, the purpose is to determine the dimensions $2a'$ and $2b'$ of $\mathscr{D}'$ able to reach a desired accuracy in approximating $\underline{E}_2$ by $\underline{E}_1$, whichever the radiated/scattered field $\underline{E}_1$ is. To this end, without loss of generality, we consider a scalar problem and introduce two operators, which we call the source operator $\mathscr{A}_1$ and the panel operator $\mathscr{A}_2$, which return the scalar fields E_1 and E_2 of interest, respectively, on $\mathscr{D}$.

A. Source Operator $\mathscr{A}_1$

On adopting a spherical harmonics field representation [27], the field E_1 on $\mathscr{D}$ can be expressed as

$$E_1(x,z) = \sum_{l=0}^{\infty}\sum_{m=-l}^{l} a_{lm} h_l^{(2)}\left(\beta\sqrt{\overline{d}^2 + x^2 + z^2}\right) Y_l^m(\theta,\phi) \tag{1}$$

where a_{lm}'s are (complex) the expansion coefficients, θ and ϕ are the angular spherical coordinates of the point $(x, \overline{d}, z)$, $Y_l^m(\theta,\phi)$'s are the spherical harmonics defined as

$$Y_l^m(\theta,\phi) = (-1)^m \sqrt{\frac{2l+1}{4\pi}\frac{(l-|m|)!}{(l+m)!}} P_l^{|m|}(\cos\theta) e^{jm\phi} \tag{2}$$

P_l^m's are the associated Legendre polynomials

$$P_l^m(r) = (-1)^m \left(1-r^2\right)^{\frac{m}{2}} \frac{d^m P_l(r)}{dr^m} \tag{3}$$

P_l's are the Legendre polynomials, and $h_l^{(2)}$'s are the spherical Hankel functions of the lth order and second kind defined as

$$h_l^{(2)}(r) = \sqrt{\frac{\pi}{2r}} H_l^{(2)}(r) \tag{4}$$

in which $H_l^{(2)}$'s are the cylindrical Hankel functions. In (1), the condition $\sqrt{\overline{d}^2 + x^2 + z^2} > a_R$ has been understood.

If βa_R is sufficiently larger than 1 and $\mathscr{D}$ is sufficiently far from $\mathscr{S}$, then (1) can be rewritten involving a finite number of terms as

$$E_1(x,z) \simeq \sum_{l=0}^{\lfloor \beta a_R \rceil}\sum_{m=-l}^{l} a_{lm} h_l^{(2)}\left(\beta\sqrt{\overline{d}^2 + x^2 + z^2}\right) Y_l^m(\theta,\phi) \tag{5}$$

where $\lfloor \xi \rceil$ is the nearest integer to ξ. Accordingly, the source operator $\mathscr{A}_1$ linking the relevant spherical harmonics coefficients to the field E_1 produced by Σ on $\mathscr{D}$ can be defined as

$$\mathscr{A}_1 \; : \; \{a_{lm}\}_{l=0,|m|\le l}^{\lfloor \beta a_R \rceil} \rightarrow \sum_{l=0}^{\lfloor \beta a_R \rceil}\sum_{m=-l}^{l} a_{lm} h_l^{(2)}\left(\beta\sqrt{\overline{d}^2 + x^2 + z^2}\right) Y_l^m(\theta,\phi). \tag{6}$$

B. Panel Operator $\mathscr{A}_2$

Similarly, we can use a representation based on the prolate spheroidal wave functions (PSWFs) [28], [29] for the current $J_{\mathscr{D}'}$ on $\mathscr{D}'$, which leads to a PSWFs expansion of the associated plane wave spectrum (PWS). In other words, the PWS $\hat{E}(k_x, k_z)$, k_x and k_z being the conjugate variables to x and z, respectively, can be written as

$$\hat{E}(k_x,k_z) = \sum_{m=0}^{\infty}\sum_{n=0}^{\infty} b_{nm} \Phi_n\left[c_x, a'\frac{k_x}{\beta}\right]\Phi_m\left[c_z, b'\frac{k_z}{\beta}\right] \tag{7}$$

where $c_x = \beta a'$, $c_z = \beta b'$, b_{nm}'s are (complex) expansion coefficients, and $\Phi_k[c_w, w]$ is the kth PSWF with space–bandwidth product equal to c_w. As before, if $\beta a'$ and $\beta b'$ are sufficiently larger than one and $\mathscr{D}$ and $\mathscr{D}'$ are sufficiently spaced, then the expansion (7) can be truncated as [28], [29]

$$\hat{E}(k_x,k_z) \simeq \sum_{m=0}^{M}\sum_{n=0}^{N} b_{nm} \Phi_n\left[c_x, a'\frac{k_x}{\beta}\right]\Phi_m\left[c_z, b'\frac{k_z}{\beta}\right] \tag{8}$$

where $N = \lfloor 4a'/\lambda \rceil$ and $M = \lfloor 4b'/\lambda \rceil$. Accordingly, if $\mathscr{D}'$ is sufficiently far from $\mathscr{D}$, the operator $\mathscr{A}_2$ linking the PSWF coefficients to the field E_2 produced by $\mathscr{D}'$ on $\mathscr{D}$ can be defined as

$$\mathscr{A}_2 \; : \; \{b_{nm}\}_{0\le n\le N}^{0\le m\le M} \rightarrow \sum_{m=0}^{M}\sum_{n=0}^{N} b_{nm} \mathscr{F}\left\{\Phi_n\left[c_x, a'\frac{k_x}{\beta}\right]\Phi_m\left[c_z, b'\frac{k_z}{\beta}\right] e^{-jk_y d}\right\} \tag{9}$$

where $\mathscr{F}$ denotes the Fourier transform operator and $k_x^2 + k_y^2 + k_z^2 = k^2$, in which k is the wavenumber.

C. Dimensioning Problem

The dimensioning problem consists of making the image of $\mathscr{A}_2$ the smallest possible one containing that of $\mathscr{A}_1$. From a practical point of view, however, strict containment is not necessary and it is sufficient that the image of $\mathscr{A}_2$ provides a good approximation of the whole image of $\mathscr{A}_1$.

In order to enforce the latter condition, we resort to the singular value expansions of $\mathscr{A}_1$ and $\mathscr{A}_2$, namely

$$\begin{cases} \mathscr{A}_1(\underline{a}) = \displaystyle\sum_{k=1}^{N^{(1)}} \sigma_k^{(1)} v_k^{(1)}(x,z)\, \underline{a}^T \cdot \underline{u}_k^{(1)*} \\ \mathscr{A}_2(\underline{b}) = \displaystyle\sum_{k=1}^{N^{(2)}} \sigma_k^{(2)} v_k^{(2)}(x,z)\, \underline{b}^T \cdot \underline{u}_k^{(2)*} \end{cases} \tag{10}$$

where $\{\sigma_k^{(i)},\ v_k^{(i)}, \underline{u}_k^{(i)}\}_{k=0}^{N^{(i)}}$ are the singular systems of $\mathscr{A}_i$, $i = 1, 2$, and $\langle\cdot,\cdot\rangle$. The functions $v_k^{(1)}(x,z)$'s expand $E_1(x,z)$, while the functions $v_k^{(2)}(x,z)$'s expand $E_2(x,z)$.

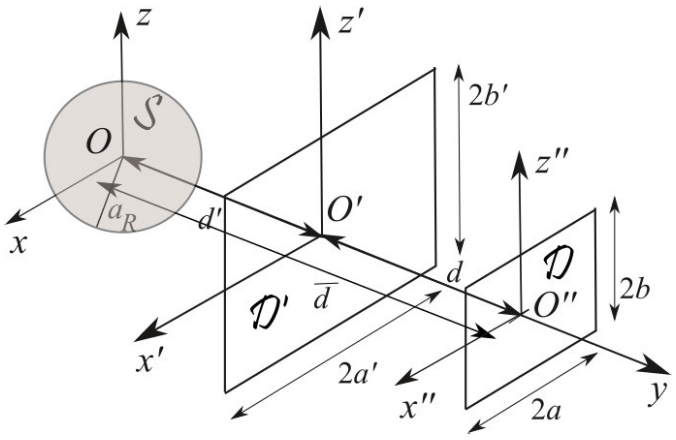

Fig. 2. Geometry of the problem.

The expansions (10) are finite-dimensional since the input spaces of operators $\mathscr{A}_1$ and $\mathscr{A}_2$ are finite-dimensional. Nevertheless, depending on the behavior of the singular values $\sigma_k^{(i)}$'s, the expansions (10) can be further truncated to $K^{(i)}$ terms, $i = 1, 2$, namely

$$\begin{cases} \mathscr{A}_1(\underline{a}) \simeq \displaystyle\sum_{k=1}^{K^{(1)}} \sigma_k^{(1)} v_k^{(1)}(x, z)\, \underline{a}^T \cdot \underline{u}_k^{(1)*} \\ \mathscr{A}_2(\underline{b}) \simeq \displaystyle\sum_{k=1}^{K^{(2)}} \sigma_k^{(2)} v_k^{(2)}(x, z)\, \underline{b}^T \cdot \underline{u}_k^{(2)*}. \end{cases} \tag{11}$$

In (11), $K^{(i)}$, $i = 1, 2$, represents the number of singular values above a prescribed threshold.

Enabling the panel $\mathscr{D}'$ to generate on $\mathscr{D}$ all the possible fields radiated/scattered by objects inside $\mathscr{S}$ requires to let the subspace $\mathscr{S}_2$ spanned by $\{v_k^{(2)}(x, z)\}_{k=1}^{K^{(2)}}$ be the smallest one containing the subspace $\mathscr{S}_1$ spanned by $\{v_k^{(1)}(x, z)\}_{k=1}^{K^{(1)}}$. Such a task can be faced by the approach discussed in the following.

III. Solution Approach

We describe the proposed approach for dimensioning the $\mathscr{D}'$ panel, i.e., for the determination of the parameters a' and b'.

We consider a generic field $E(x, z)$ that can be radiated/scattered by objects within the sphere $\mathscr{S}$. In other words, the following approximation for E is possible

$$E(x, z) = \sum_{p=1}^{K^{(1)}} c_p v_p^{(1)}(x, z). \tag{12}$$

Being the interest in relative errors, we suppose that E has unit norm, namely, $\|E\|^2_{\mathscr{L}^2(\mathscr{D})} = 1$.

The best approximation of E radiated by $\mathscr{D}'$ is its projection $E^{(Pr)}$ onto $\mathscr{S}_2$, namely

$$E^{(Pr)}(x, z) = \sum_{q=1}^{K^{(2)}} d_q v_q^{(2)}(x, z) \tag{13}$$

where $d_q = \langle E, v_q^{(2)} \rangle_{\mathscr{L}^2(\mathscr{D})}$ and $\langle \cdot, \cdot \rangle_{\mathscr{L}^2(\mathscr{D})}$ is the scalar product in the space $\mathscr{L}^2(\mathscr{D})$ of square integrable functions on $\mathscr{D}$. The mean square error committed by the approximation (13) is

$$\mathscr{E}^2(\underline{c}; a', b') = \left\| E - E^{(Pr)} \right\|^2_{\mathscr{L}^2(\mathscr{D})} \tag{14}$$

where $\underline{c}$ is the $K^{(1)} \times 1$ column vector of the c_p's and $\|\cdot\|_{\mathscr{L}^2(\mathscr{D})}$ is the norm in $\mathscr{L}^2(\mathscr{D})$ and where the dependence of $\mathscr{E}$ from the unknown problem parameters a' and b' has been highlighted. Notice that, being $\|E\|^2_{\mathscr{L}^2(\mathscr{D})} = 1$, the error in (14) is also a relative one.

It can be seen (see the Appendix) that the squared error $\mathscr{E}^2$ can be written as

$$\mathscr{E}^2(\underline{c}; a', b') = 1 - \underline{c}^H \, \underline{\underline{A}} \, \underline{c} \tag{15}$$

where ^{H} denotes the conjugate transposition and $\underline{\underline{A}}$ is a $K^{(1)} \times K^{(1)}$ matrix having the following generic element:

$$A_{mn} = \sum_{q=1}^{K^{(2)}} \langle v_m^{(1)}, v_q^{(2)} \rangle_{\mathscr{L}^2(\mathscr{D})} \langle v_q^{(2)}, v_n^{(1)} \rangle_{\mathscr{L}^2(\mathscr{D})} \tag{16}$$

with * expressing complex conjugation. Straightforwardly, $A^*_{mn} = A_{nm}$, and $\underline{\underline{A}}$ is Hermitian.

It should be noticed that, having assumed E of unit norm, the same property holds true also for the coefficients $\underline{c} = (c_1, c_2, \ldots, c_{K^{(1)}})$, namely, $\|\underline{c}\|^2 = 1$, where $\|\underline{c}\|^2 = |c_1|^2 + |c_2|^2 + \cdots + |c_{K^{(1)}}|^2$. The relative error (15) has thus definition domain on the surface of a $K^{(1)}$-dimensional unit ball.

The quantity $\underline{c}^H \, \underline{\underline{A}} \, \underline{c}$ is a quadratic form defined on a Hermitian matrix $\underline{\underline{A}}$ and is then real. Furthermore, we can easily prove that such a quadratic form is positive semidefinite. Indeed, the field E can be decomposed as

$$E = E^{(Pr)} + E^{(O)} \tag{17}$$

where $E^{(O)}$ represents the projection of E on the subspace orthogonal to $\mathscr{S}_2$. For this reason,

$$\mathscr{E}^2(\underline{c}; a', b') = \left\| E^{(O)} \right\|^2_{\mathscr{L}^2(\mathscr{D})}. \tag{18}$$

Being $\|E\|^2_{\mathscr{L}^2(\mathscr{D})} = 1$, then $\left\| E^{(O)} \right\|^2_{\mathscr{L}^2(\mathscr{D})} \leq 1$ and so

$$\mathscr{E}^2(\underline{c}; a', b') \leq 1. \tag{19}$$

By comparing (19) and (15), it is possible to deduce that

$$\underline{c}^H \, \underline{\underline{A}} \, \underline{c} \geq 0 \quad \forall \underline{c}, \text{ with } \|\underline{c}\|^2 = 1. \tag{20}$$

It makes thus sense to determine the maximum error committed by varying the coefficients $\underline{c}$ on the unit ball. The maximum error $\mathscr{E}^2$ on the unit ball is then reached in correspondence to the minimum of $\underline{c}^H \, \underline{\underline{A}} \, \underline{c}$. Since $\underline{\underline{A}}$ is Hermitian, the eigenvalues e_n are real. The minimum of the quadratic form at hand on the unit ball is equal to the minimum e_{min} of such eigenvalues. The maximum square error is so

$$\mathscr{E}^2_{max}(a', b') = \max_{\|\underline{c}\|^2 = 1} \mathscr{E}(\underline{c}; a', b') = 1 - e_{min}. \tag{21}$$

We notice that Fourier transform relations are useful to evaluate, in a fast way, input–output operator relations when geometry allows. For the geometry considered in this article, it has been possible to exploit the assumptions of a flat panel and targeted regions to enable the fast evaluation of the panel

operator by using the Fourier transform relation involved in the PWS representation. In particular, the fast Fourier transform (FFT) algorithm has been adopted. On the other side, our formulation relies on the capability of the SVD to provide the essential part of the involved operators as well as their essential input and output spaces regardless of shape and size of the involved domains.

Here, for the sake of simplicity, we will assume a square domain $\mathscr{D}$, namely, $a = b$, so that we guess that also the optimal radiating panel is square, namely, $a' = b'$, due to the system symmetry. Moreover, we assume that the maximum square error $\mathscr{E}^2_{max}(a')$ reduces for an increasing a'. Indeed, for an increasing a', the size of the space of the fields radiated by $\mathscr{D}'$ increases and we expect that the subspace spanned by $\{v_k^{(2)}(x,z)\}_{k=1}^{K^{(2)}}$ "includes" even better the subspace spanned by $\{v_k^{(1)}(x,z)\}_{k=1}^{K^{(1)}}$. We expect also that the decrease in $\mathscr{E}^2_{max}(a')$ with a' is monotonic.

The practical determination of the optimal size a' is obtained as the smallest value a' making

$$\mathscr{E}^2_{max}(a') \leq \overline{\mathscr{E}}^2_{max} \tag{22}$$

where $\overline{\mathscr{E}}^2_{max}$ is a maximum tolerable square error.

The concept of angle between subspaces resounds the approach used in this article, but our approach is the effective one to guarantee the prefixed tolerance. According to the definition by Risteski and Trenčevski [30] and Zhua and Knyazev [31], the determinant of matrix $\underline{\underline{A}}$ coincides with $\cos^2\theta$, where θ is the angle between the two subspaces $\mathscr{S}_1$ and $\mathscr{S}_2$. In [30], it is also shown that $det(\underline{\underline{A}})$ is the product of the eigenvalues.

The aim of our approach is defining a radiating panel so that $\mathscr{S}_1$ is in fact a subspace of $\mathscr{S}_2$, but, to achieve this goal, we are maximizing the minimum eigenvalue of $\underline{\underline{A}}$. We are thus not targeting a condition of vanishing angle between the two subspaces $\mathscr{S}_1$ and $\mathscr{S}_2$ and minimizing the angle between $\mathscr{S}_1$ and $\mathscr{S}_2$ does just something similar to our procedure.

Once designed the dimensions of the radiating panel $\mathscr{D}'$, the problem arises of determining the current distribution supported on $\mathscr{D}'$ capable to radiate the same field of the radiator/scatterer located within the sphere $\mathscr{S}$.

Once assigned the field radiated/scattered on $\mathscr{D}$, the inverse problem of determining $J_{\mathscr{D}'}$ and, in particular, the PSWFs coefficients b_{nm}'s, can be solved in a regularized way by a truncated SVD of $\mathscr{A}_2$ [5], [6].

In this article, a continuous radiating panel $\mathscr{D}'$ is considered. Guidelines for its discretization have been provided in [8] and [13].

Finally, we stress that the number of significant singular values of the two operators $\mathscr{A}_1$ and $\mathscr{A}_2$, namely, $K^{(1)}$ and $K^{(2)}$, represents the essential dimensions of their respective output subspaces $\mathscr{S}_1$ and $\mathscr{S}_2$ that are embedded in a larger space. We observe that an equal dimensionality of the two subspaces does not guarantee that they are close to each other so that comparing the two essential dimensions $K^{(1)}$ and $K^{(2)}$ should be better regarded as an order relation and attempting to balance $K^{(1)}$ and $K^{(2)}$ is not diriment. We also stress that we are actually not demanding that $\mathscr{S}_1$ and $\mathscr{S}_2$ are essentially the same, which would be a too strong request. We are instead requiring that the output space of the panel operator contains that of the source operator. This request is weaker since $\mathscr{S}_2$ is enabled to show more vector directions than $\mathscr{S}_1$. In other words, acceptable solutions to the problem include cases when the equivalent panel radiates also along functional directions orthogonal to those of the primary source. Obviously, once $\mathscr{S}_2 \supseteq \mathscr{S}_1$, requiring that $K^{(2)}$ gets closer to $K^{(1)}$ becomes desirable. Furthermore, the condition $K^{(1)} \simeq K^{(2)}$ is not sufficient to guarantee that $\mathscr{S}_2 \supseteq \mathscr{S}_1$.

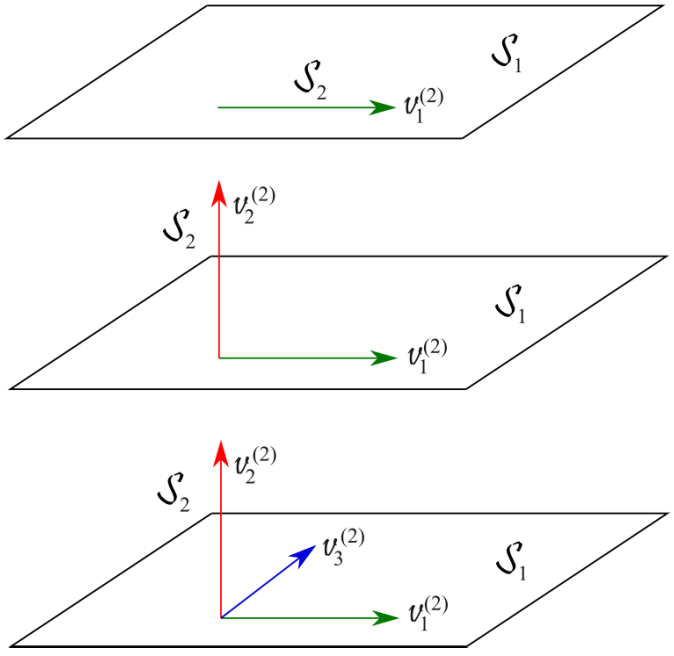

Fig. 3. Illustrating how the condition $\mathscr{S}_2 \supseteq \mathscr{S}_1$ is reached during the panel dimensioning.

The order relation between $K^{(1)}$ and $K^{(2)}$ is exemplified in Fig. 3 in which $K^{(1)} = 2$. Suppose that, for an initial panel size, the range of $\mathscr{A}_2$ is given by the only vector $v_1^{(2)} \subset \mathscr{S}_1$ so that $\mathscr{S}_2 \subset \mathscr{S}_1$. Suppose now that, by increasing the panel size, the new vector $v_2^{(2)}$, orthogonal to $\mathscr{S}_1$, appears in the range of $\mathscr{A}_2$. This situation is still not sufficient to guarantee that $\mathscr{S}_2 \supseteq \mathscr{S}_1$, notwithstanding now $K^{(1)} = K^{(2)}$. Assume finally that, by increasing again the panel size, the new vector $v_3^{(2)}$ appears in the range of $\mathscr{A}_2$. We can now stop increasing the panel size since $\mathscr{S}_2 \supset \mathscr{S}_1$. Nevertheless, $K^{(2)} > K^{(1)}$ since the vector $v_2^{(2)}$ is useless to our purposes.

It should be noticed that, although the dimensioning can lead to $K^{(2)} > K^{(1)}$ and $\mathscr{S}_2 \supset \mathscr{S}_1$, a degree of freedom is, however, left to the design stage of the secondary source. Indeed, the secondary source will be requested to excite only $v_1^{(2)}$ and $v_3^{(2)}$ and not also $v_2^{(2)}$.

IV. Numerical Results

In this section, we present numerical results to assess the performance of the approach.

First, we illustrate the panel dimensioning. Later on, we consider three different test cases in which one or more objects present within the sphere $\mathscr{S}$ scatter an impinging field. All the three cases share the same dimensioned panel,

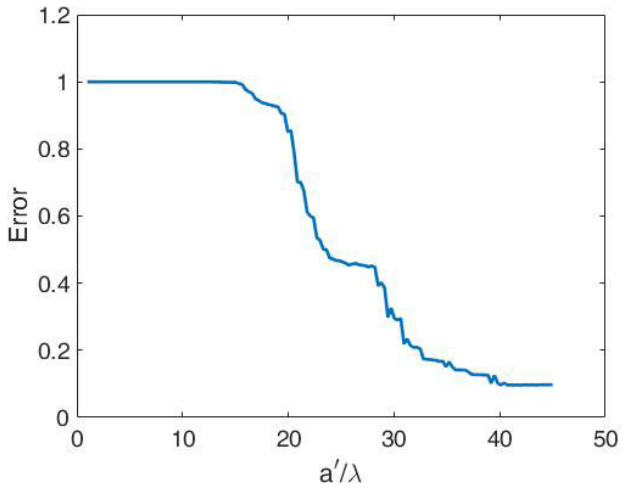

Fig. 4. Dimensioning. Error curve for different values of $a'/\lambda = b'/\lambda$.

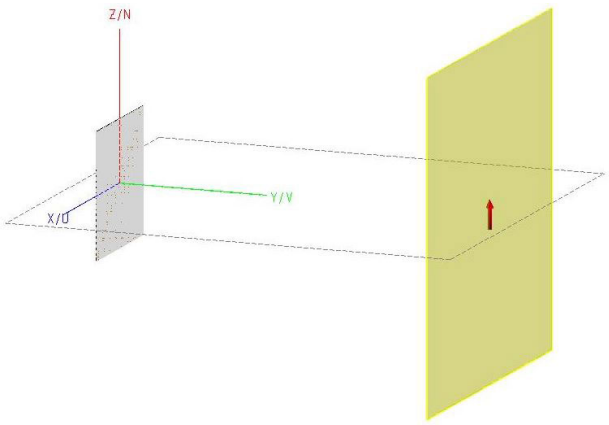

Fig. 5. Case #1. FEKO view of the scattering plate case. Left: scattering plate is pictured in gray. Right: domain $\mathscr{D}$ is displayed in ocra and the illuminating elementary dipole is also visible.

while the panel excitation synthesis changes depending on the scatterers contained in $\mathscr{S}$.

In this article, without loss of generality, we address scattering cases from perfectly electric conducting objects only instead of radiation ones. In all the test cases, when performing the inversions of operator $\mathscr{A}_2$, its singular values have been cut at a level of 40 dB below their maximum one. Furthermore, for all the test cases, the reference fields have been generated by Altair FEKO.

A. Panel Dimensioning

Concerning the panel dimensioning, the sphere $\mathscr{S}$ has been assumed having radius 4λ, and the region $\mathscr{D}$ has been supposed to have dimensions $a = b = 7.5\lambda$, while the spacings d' and $\overline{d}$ have been set to 7λ and 17λ, respectively. In Fig. 4, the error curve $\mathscr{E}_{max}$ is reported against $a'/\lambda = b'/\lambda$. As it can be seen, the error keeps less or equal to 1, as expected. Moreover, the function $\mathscr{E}_{max}(a')$ is decreasing. On assuming a (relative) maximum error of 0.1 acceptable, then the minimum size of the radiating panel $a' = b'$ is 40λ. Therefore, in all the test cases that will be presented in the following, a panel as large as $40\lambda \times 40\lambda$ will be considered.

We notice that the value of 40λ for a' and b' is significantly larger than that of a and b due to the relatively large values considered for d' and d.

Theoretically, $\mathscr{D}'$ and $\mathscr{D}$ can be arbitrarily close, provided that the reactive contributions to the field radiated by $\mathscr{D}'$ on $\mathscr{D}$ are considered.

However, in practical applications, $\mathscr{D}'$ must be physically realized: it will represent a real radiator under the aperture modeling and its mutual coupling with probes or devices under test located in $\mathscr{D}$ may arise and should be possibly avoided or considered.

In order to refer to a practical application, let us consider the automotive [9], [10] case in which the radiating panel should be capable to radiate the field scattered by different kinds of objects (pedestrians, bicycles, cars, and so on) on the radar sensor. Obviously, in the case when the radiating panel is chosen very close to the radar sensor, the effect of the mutual coupling should be explicitly considered and handled.

Similarly, also, $\mathscr{S}$ and $\mathscr{D}'$ can be arbitrarily close. However, when both are very close to $\mathscr{D}$, again, the reactive contributions to the field radiated by $\mathscr{S}$ and $\mathscr{D}'$ on $\mathscr{D}$ should be considered.

Finally, due to the arbitrariness of the position of $\mathscr{D}'$, the devised approach can also be employed to define the best panel position according to prefixed criteria.

We also notice that our approach pursues a general purpose, and in this article, we analyze the problem principles. Depending on the need, the radiating panel can be set closer and sized smaller if a larger error can be tolerated.

B. Case #1: Plate

Following the panel dimensioning, as a first test case, we consider that of a square perfectly conducting plate inscribed within a sphere of radius 4λ (see Fig. 5). Testing the performance of the approach in this case is of interest being the plate a canonical scatterer. The plate has a side of $8/\sqrt{2}\lambda$. In all the following simulations, the scatterers are illuminated by an elementary dipole located at the center of $\mathscr{D}$ and oriented along the y-axis.

In Figs. 6 and 7, the amplitude and phase of the current distribution on $\mathscr{D}'$ is displayed. As it can be seen, the field is significant and the phase is approximately constant in the region of the radiating panel just in front of the plate.

From Fig. 8, it is possible to compare the amplitude and phase of the field scattered by the plate with that radiated by the panel at hand. The capability of the radiating panel of reproducing such a scattered field with high accuracy can be better appreciated by the field cuts along x and y in Figs. 9 and 10, respectively. The percentage error experienced while reproducing the scattered field with that radiated by $\mathscr{D}'$ has been 0.03%, well below the previously considered, maximum tolerated error. In other words, 0.1 is just the maximum relative mean square error, while there are many possible fields in the set of fields radiated/scattered by the sources/scatterers that correspond to lower errors.

C. Case #2: Many Spheres

Let us consider now a scatterer more complex than the previously considered one. More in detail, we address the case

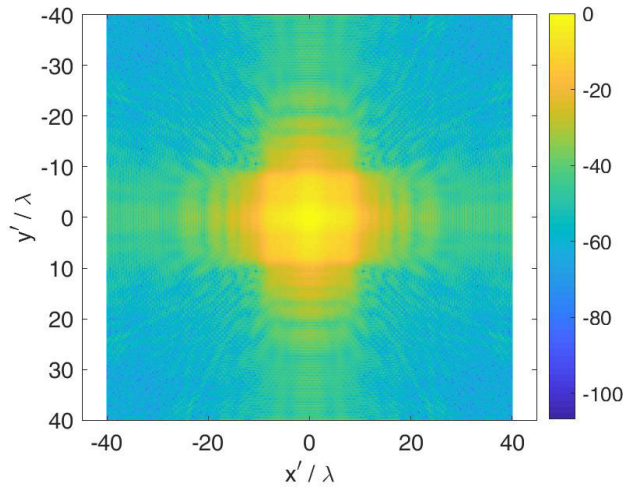

Fig. 6. Case #1. Amplitude of the synthesized current distribution on $\mathscr{D}'$ for the plate case.

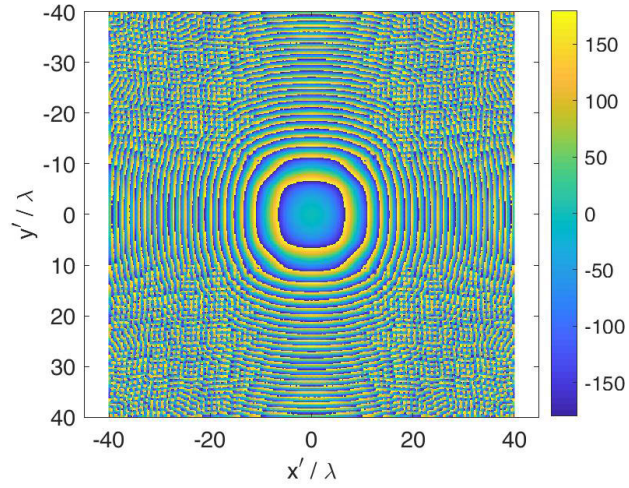

Fig. 7. Case #1. Phase of the synthesized current distribution on $\mathscr{D}'$ for the plate case.

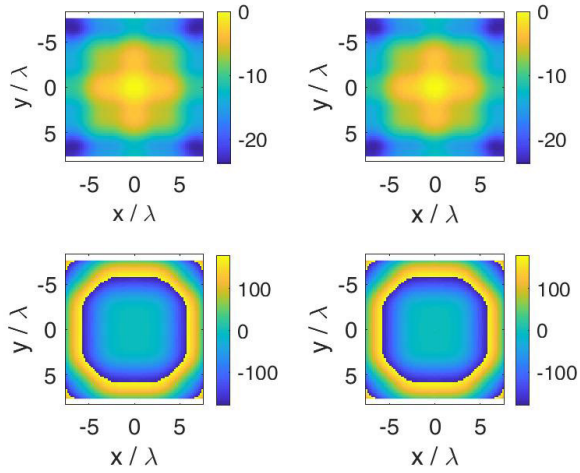

Fig. 8. Case #1. Amplitude and phase of the field on $\mathscr{D}$. Left: field radiated by $\mathscr{D}'$. Right: field scattered by the plate inscribed in $\mathscr{S}$.

of an aggregate of 24 small spheres having radius $\lambda/10$ and randomly located within $\mathscr{S}$ (see Fig. 11).

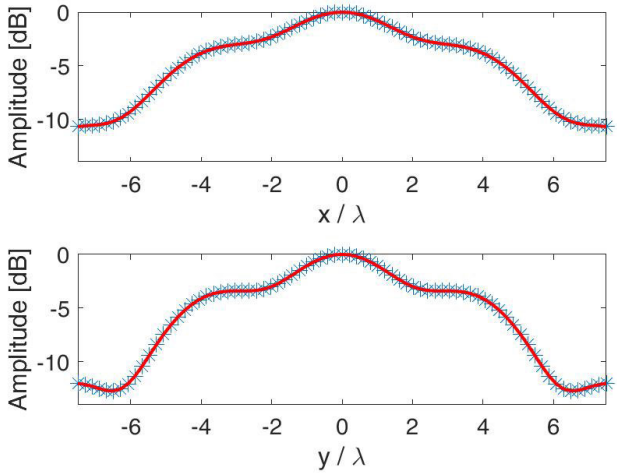

Fig. 9. Case #1. Cut, along the x-axis, of the field amplitude radiated by $\mathscr{D}'$ (red line) and scattered by the plate (blue asterisks).

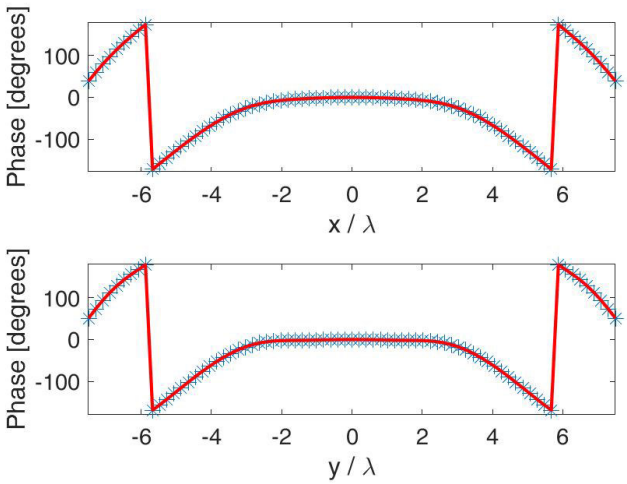

Fig. 10. Case #1. Cut, along the x-axis, of the field phase radiated by $\mathscr{D}'$ (red line) and scattered by the plate (blue asterisks).

In Figs. 12 and 13, the amplitude and phase of the current distribution on $\mathscr{D}'$ is depicted. As appreciable, the field is significant in the region of the radiating panel just in front of the scattering spheres.

From Fig. 14, it is possible to compare the amplitude and phase of the field scattered by the aggregated spheres with that radiated by the panel in question. The ability of the radiating panel of reproducing such a scattered field with high accuracy can be better appreciated by the cuts along x and y in Figs. 15 and 16, respectively. The percentage error committed while reproducing the scattered field with that radiated by $\mathscr{D}'$ has been equal to 0.12%, once again well below the maximum tolerated error.

We finally notice that, following our procedure, the space of the fields that can be radiated by the primary source is fully represented, within the prescribed accuracy, by those radiated by the panel. Thus, the method will also work when only the sidelobes of the field radiated by the primary source are observed in $\mathscr{D}$. From this point of view, we remark that the present test case #2 has been constructed to have an intense field also outside the domain $\mathscr{D}$ and so to prove that the approach works well when the field radiated by the

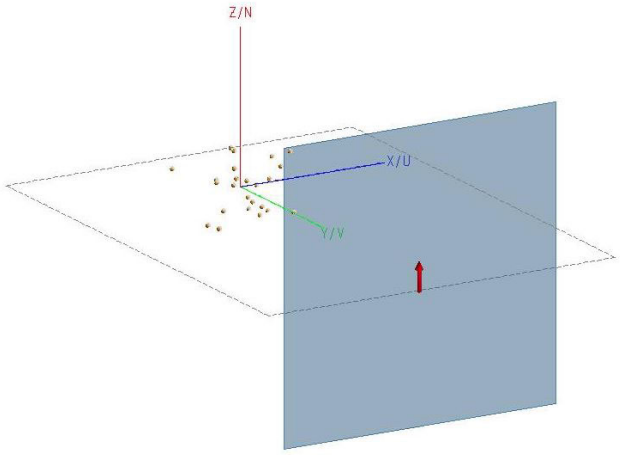

Fig. 11. Case #2. FEKO view of the scattering spheres aggregate case. On the left, 24 spheres having a radius equal to $\lambda/10$ randomly positioned in $\mathscr{S}$. On the right, the domain $\mathscr{D}$ is displayed in ocra and the illuminating elementary dipole is also visible.

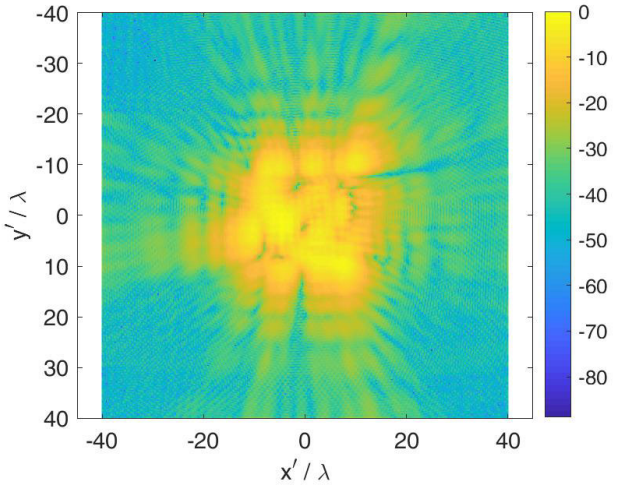

Fig. 12. Case #2. Amplitude of the synthesized current distribution on $\mathscr{D}'$ for the many spheres case.

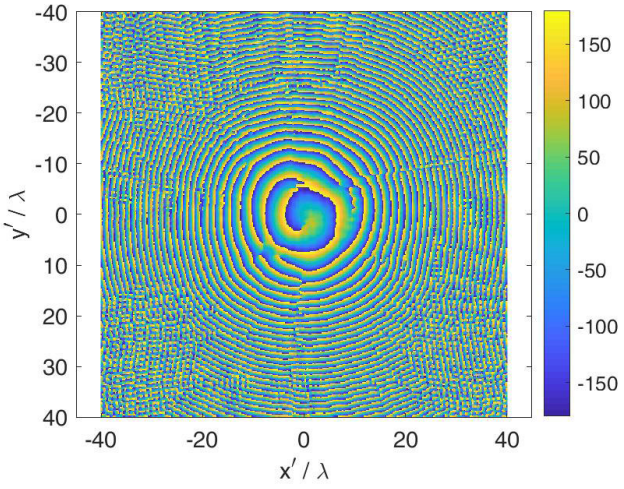

Fig. 13. Case #2. Phase of the synthesized current distribution on $\mathscr{D}'$ for the many spheres case.

source/scatterer is essentially confined to $\mathscr{D}$ as in cases #1 and #3, see also the following.

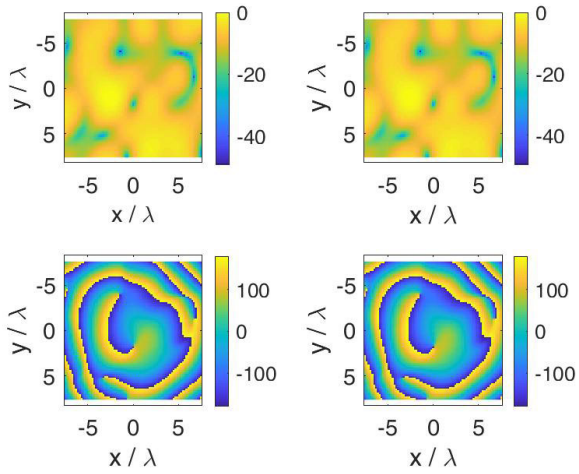

Fig. 14. Case #2. Amplitude and phase of the field radiated on $\mathscr{D}$. Left: field radiated by $\mathscr{D}'$. Right: field scattered by the spheres aggregate.

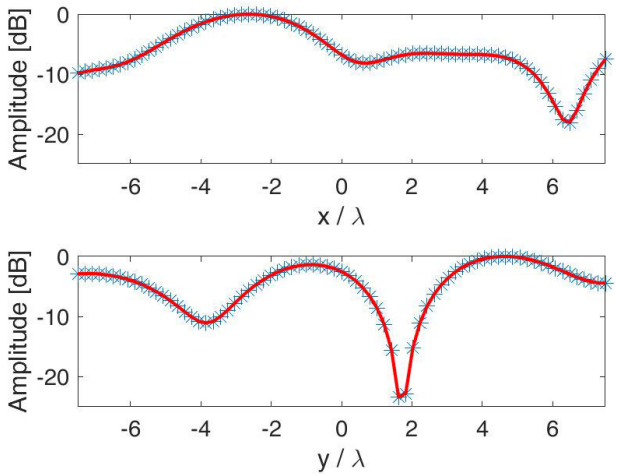

Fig. 15. Case #2. Cut, along the x-axis, of the field amplitude radiated by $\mathscr{D}'$ (red line) and scattered by the spheres aggregate (blue asterisks).

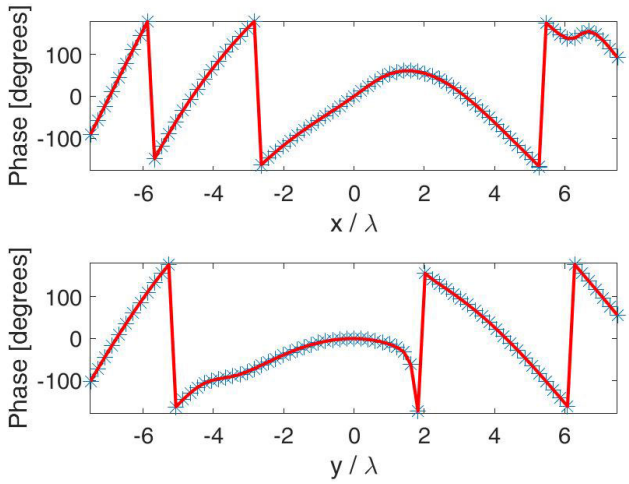

Fig. 16. Case #2. Cut, along the x-axis, of the field phase radiated by $\mathscr{D}'$ (red line) and scattered by the spheres aggregate (blue asterisks).

D. Case #3: Solitary Sphere

Let us conclude the numerical cases by considering that of a solitary sphere of radius 4λ (see Fig. 17). This case

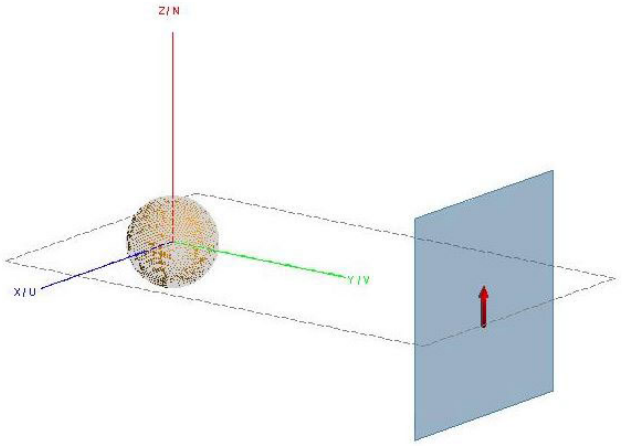

Fig. 17. Case #3. FEKO view of the scattering sphere case. On the left, 24 spheres having radius equal to $\lambda/10$ randomly positioned in $\mathscr{S}$. On the right, the domain $\mathscr{D}$ is displayed in ocra and the illuminating elementary dipole is also visible.

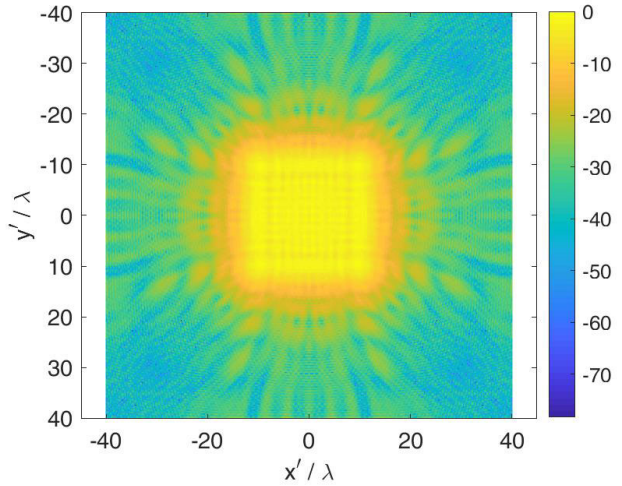

Fig. 18. Case #3. Amplitude of the synthesized current distribution on $\mathscr{D}'$ for the solitary sphere case.

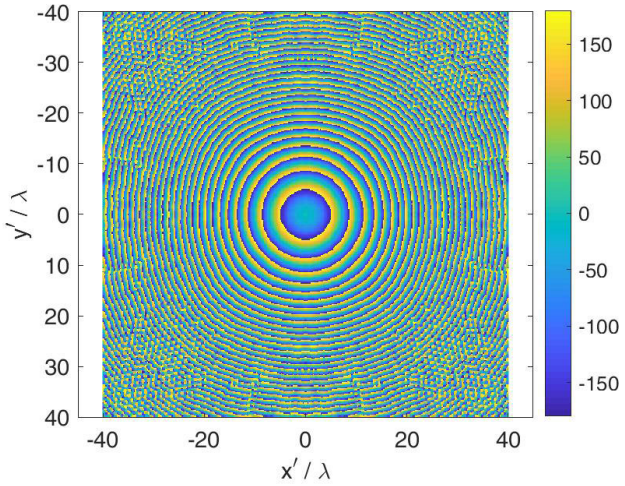

Fig. 19. Case #3. Phase of the synthesized current distribution on $\mathscr{D}'$ for the solitary sphere case.

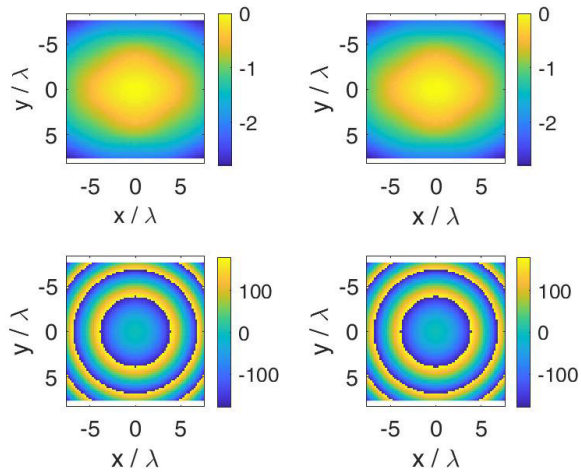

Fig. 20. Case #3. Amplitude and phase of the field radiated on $\mathscr{D}$. Left: field radiated by $\mathscr{D}'$. Right: field scattered by the solitary sphere.

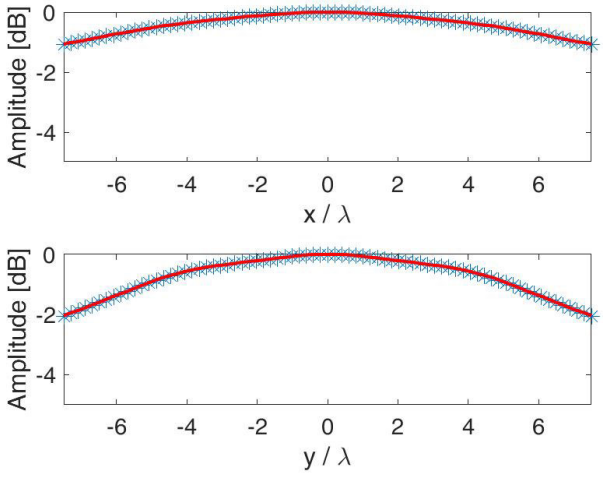

Fig. 21. Case #3. Cut, along the x-axis, of the field amplitude radiated by $\mathscr{D}'$ (red line) and scattered by the solitary sphere (blue asterisks).

is presented since the sphere gives rise to a scattered field receiving only a weak tapering in $\mathscr{D}$, thus representing a difficult test case.

In Figs. 18 and 19, the amplitude and phase of the current distribution on $\mathscr{D}'$ are illustrated by highlighting, once again, that the field is significant on the region of the radiating panel just in front of the sphere.

From Fig. 20, it is possible to compare the amplitude and phase of the field scattered by the sphere with that radiated by the panel at hand. The capability of the radiating panel of reproducing such a scattered field with high accuracy can be better appreciated by the cuts of such fields along x and y in Figs. 21 and 22, respectively. The percentage error committed in reproducing the scattered field has been equal to 0.10%, much below the maximum tolerated error.

E. Reducing the Panel Size

In this section, we shortly highlight how the performance of the approach degrades for a diminishing size of the radiating panel for the three, previously considered cases, namely, plate, many spheres, and solitary sphere. In particular, in Fig. 23, we show how the percentage error between the reference and radiated field fastly grows when the panel size is reduced. It has been highlighted [8] how, for the targeted applications,

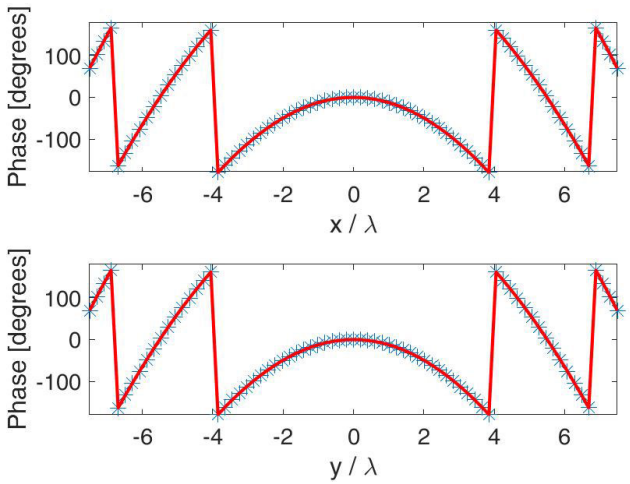

Fig. 22. Case #3. Cut, along the x-axis, of the field phase radiated by $\mathscr{D}'$ (red line) and scattered by the solitary sphere (blue asterisks).

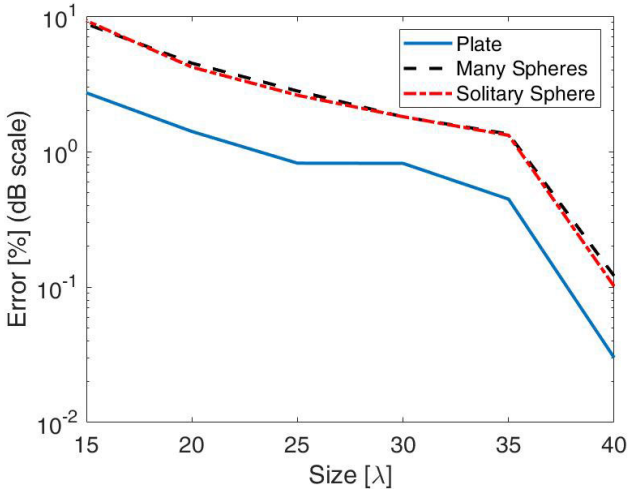

Fig. 23. Percentage errors (in a decibel scale) for different sizes of the radiating panel.

having an accurate reproduction of the near field is particularly relevant.

F. Results for a Radiating Panel Closer to the Radiator/Scatterer

In this section, we show the performance of the approach for a radiating panel located closer to the radiator/scatterer than before. In other words, we consider a smaller value of $d' = 5\lambda$, the other system parameters being unchanged. On assuming once again a (relative) maximum error of 0.1 acceptable, then the minimum size of the radiating panel $a' = b'$ has been 30λ, smaller than previously.

Furthermore, we address again the case of the aggregate of the 24 small spheres. In Figs. 24 and 25, the amplitude and phase of the current distribution on $\mathscr{D}'$ are depicted. Also, from Figs. 26 and 27, the cuts along x and y of amplitude and phase, respectively, of the field scattered by the aggregated spheres can be compared to those radiated by the panel in question, showing again a satisfactory agreement.

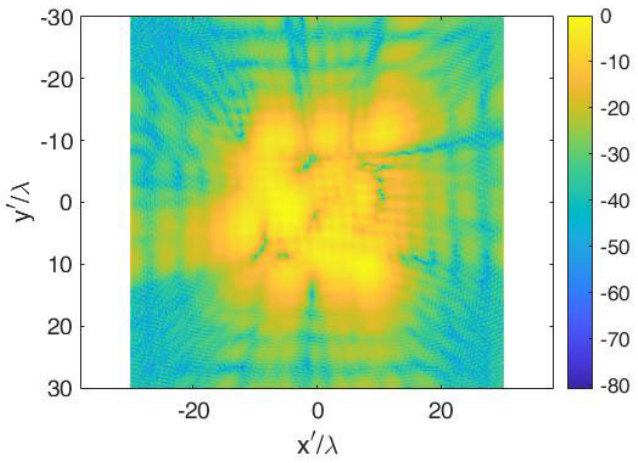

Fig. 24. Closer radiator case with many spheres. Amplitude of the synthesized current distribution on $\mathscr{D}'$.

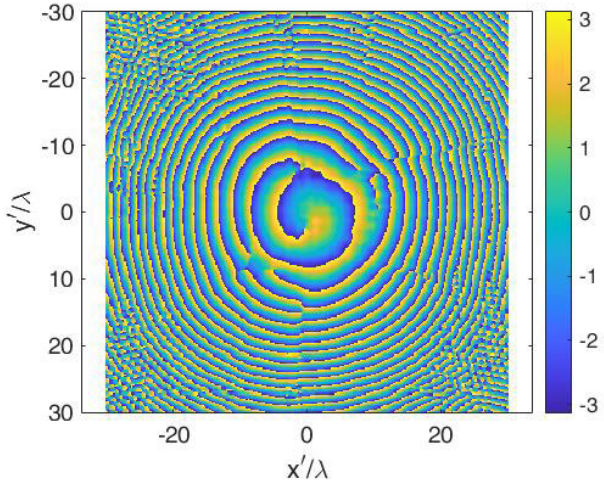

Fig. 25. Closer radiator case with many spheres. Phase of the synthesized current distribution on $\mathscr{D}'$.

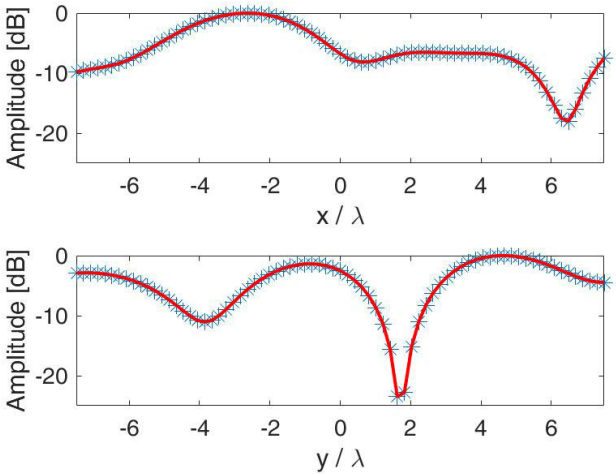

Fig. 26. Closer radiator case with many spheres. Cut, along the x-axis, of the field amplitude radiated by $\mathscr{D}'$ (red line) and scattered by the many spheres (blue asterisks).

The percentage error committed while reproducing the scattered field with that radiated by $\mathscr{D}'$ has been equal to 0.11%, once again well below the maximum.

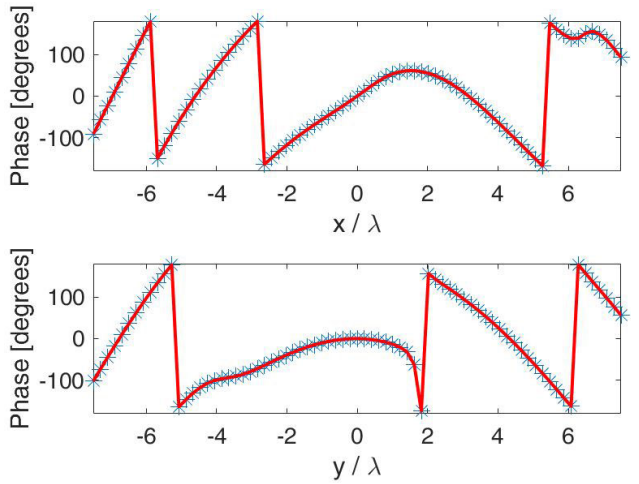

Fig. 27. Closer radiator case with many spheres. Cut, along the x-axis, of the field phase radiated by $\mathscr{D}'$ (red line) and scattered by the many spheres (blue asterisks).

We finally notice that approaching the domain $\mathscr{D}$ to the radiators/scatterers would not produce a size reduction of $\mathscr{D}'$ as well since the radiating panel would be appointed to reproduce a proper number of degrees of freedom.

V. Conclusion

We have tackled the problem of modeling a radiator or a scatterer using an equivalent radiator. Having prefixed the shape of the equivalent radiator, we have introduced an approach for the solution of such sizing issue.

The approach relies on the use of the SVD of the operators linking the radiator/scatterer to the field on the region of interest and the equivalent radiating panel to the field on the same domain. The singular functions of such operators corresponding to the most significant singular values represent the spaces to which the fields radiated by the primary radiator/scatterer and that radiated by the equivalent one essentially belong. The approach consists of determining the dimensions of the equivalent radiator minimizing the error by which the field radiated on $\mathscr{D}$ by the equivalent radiator approximates the primary radiated/scattered one. The error is expressed as a Hermitian, definite positive quadratic form so that the problem amounts to the maximization of its minimum eigenvalue.

Having introduced the approach for the first time, in this article, we have considered the particular case of rectangular panel and focused the attention on the dimensioning problem. In the future, we will deal with the generalization of the method to the determination of the optimal panel shape also.

We explicitly mention that the approach can be easily extended to other kinds of problems whenever a linear formulation is possible. In particular, it can be applied to problems involving partially coherent or totally incoherent sources or scatterers.

Simulated results have been shown for an equivalent, planar radiator of rectangular shape. The radiating panel has been dimensioned to keep the maximum relative square error below 0.1. Three test cases have been considered: a solitary plate, an aggregate of electrically small spheres, and a solitary sphere. In all the cases, the error committed by the radiating panel has resulted significantly smaller than the targeted maximum error.

In this article, we have considered a "continuous" radiating panel. Discretizations of such panel can be obtained by using Gaussian quadrature or the singular value optimization (SVO) approach using the guidelines in [8] and [13].

The exploitation of the proposed approach to dimension a radiating panel capable to produce, in a quiet-zone region, tilted plane waves with tilt angle within a preassigned cone will be subject of future investigations. Also, we plan to investigate the use of different normed spaces, e.g., Sobolev spaces instead of $\mathscr{L}^2$ spaces, to embed the error evaluations.

Appendix
Representation Error Expressed as a Quadratic Form

After having decomposed the generic field E that can be radiated/scattered by objects within the sphere $\mathscr{S}$ as

$$E = E^{(Pr)} + E^{(O)} \tag{23}$$

where $E^{(Pr)}$ is the projection of E onto $\{v_n^{(2)}(x,z)\}_{n=0}^{K^{(2)}}$ and $E^{(O)}$ is its projection on the subspace orthogonal to $\{v_n^{(2)}(x,z)\}_{n=0}^{K^{(2)}}$, then the error $\mathscr{E}^2(\underline{c};a',b')$ can be rewritten as

$$\mathscr{E}^2(\underline{c};a',b') = 1 - \left\|E^{(Pr)}\right\|^2 \tag{24}$$

having observed that $\langle E^{(Pr)}, E^{(O)}\rangle = 0$ and having exploited the condition $\|E\| = 1$. Here, the subscript $\mathscr{L}^2(\mathscr{D})$ of the norm and the scalar product is being dropped for ease of notation.

According to (13), $\|E^{(Pr)}\|^2$ can be written as

$$\left\|E^{(Pr)}\right\|^2 = \sum_{q=1}^{K^{(2)}} |d_q|^2 = \left\|\underline{d}\right\|_2^2 \tag{25}$$

where $\|\cdot\|_2$ denotes the squared norm for the sequences and $\underline{d} = (d_1, d_2, \ldots, d_{K^{(2)}})$.

Since, from the definition of the d_q's, we have that

$$d_q = \sum_{p=1}^{K^{(2)}} c_p \langle v_p^{(1)}, v_q^{(2)}\rangle \tag{26}$$

then

$$\|\underline{d}\|^2 = \sum_{p',p''=1}^{K^{(2)}} c_{p'} c_{p''}^* \langle v_{p'}^{(1)}, v_q^{(2)}\rangle \langle v_q^{(2)}, v_{p''}^{(1)}\rangle \tag{27}$$

so that

$$\left\|E^{(P)}\right\|^2 = \sum_{p',p''=1}^{P} c_{p'} c_{p''}^* A_{p'p''} \tag{28}$$

where

$$A_{p'p''} = \sum_{q=1}^{K^{(2)}} \langle v_{p'}^{(1)}, v_q^{(2)}\rangle \langle v_q^{(2)}, v_{p''}^{(1)}\rangle \tag{29}$$

is the generic element of the $K^{(1)} \times K^{(1)}$, Hermitian matrix $\underline{\underline{A}}$. Accordingly, on defining $\underline{c} = (c_1, c_2, \ldots, c_{K^{(1)}})$, (28) can be written as

$$\left\| E^{(P)} \right\|^2 = \underline{c}^H \, \underline{\underline{A}} \underline{c} \tag{30}$$

and so

$$\mathscr{E}^2(\underline{c}; a', b') = 1 - \underline{c}^H \, \underline{\underline{A}} \underline{c}. \tag{31}$$

REFERENCES

[1] O. Bucci, G. Franceschetti, and G. D'Elia, "Fast analysis of large antennas—A new computational philosophy," *IEEE Trans. Antennas Propag.*, vol. AP-28, no. 3, pp. 306–310, May 1980.

[2] A. Capozzoli, C. Curcio, A. Liseno, and G. Toso, "Fast, phase-only synthesis of aperiodic reflectarrays using NUFFTS and CUDA," *Prog. Electromagn. Res.*, vol. 156, pp. 83–103, 2016.

[3] O. M. Bucci, A. Capozzoli, and G. D'Elia, "Power pattern synthesis of reconfigurable conformal arrays with near-field constraints," *IEEE Trans. Antennas Propag.*, vol. 52, no. 1, pp. 132–141, Jan. 2004.

[4] A. Capozzoli, C. Curcio, G. D'Elia, and A. Liseno, "Fast phase-only synthesis of conformal reflectarrays," *IET Microw., Antennas Propag.*, vol. 4, no. 12, p. 1989, 2010.

[5] A. Capozzoli et al., "A probe-compensated helicoidal NF-FF transformation for aperture antennas using a prolate spheroidal expansion," *Int. J. Antennas Propag.*, vol. 2012, pp. 1–13, Jan. 2012, doi: 10.1155/2012/753156.

[6] A. Capozzoli, C. Curcio, G. D'Elia, and A. Liseno, "Millimeter-wave phaseless antenna characterization," *IEEE Trans. Instrum. Meas.*, vol. 57, no. 7, pp. 1330–1337, Jul. 2008.

[7] J.-R. Regue, M. Ribo, J.-M. Garrell, and A. Martin, "A genetic algorithm based method for source identification and far-field radiated emissions prediction from near-field measurements for PCB characterization," *IEEE Trans. Electromagn. Compat.*, vol. 43, no. 4, pp. 520–530, Nov. 2001.

[8] A. Capozzoli, C. Curcio, and A. Liseno, "Time-harmonic echo generation," *IEEE Trans. Antennas Propag.*, vol. 59, no. 9, pp. 3234–3245, Sep. 2011.

[9] C. J. Rocha, R. Ribeiro, P. M. Cruz, and P. Viana, "Automatized solution for over-the-air (OTA) testing and validation of automotive radar sensors," in *Proc. IEEE-APS Topical Conf. Antennas Propag. Wireless Commun. (APWC)*, Granada, Spain, Sep. 2019, pp. 370–374.

[10] D. J. Belgiovane, C.-C. Chen, S. Y.-P. Chien, and R. Sherony, "Surrogate bicycle design for millimeter-wave automotive radar pre-collision testing," *IEEE Trans. Intell. Transp. Syst.*, vol. 18, no. 9, pp. 2413–2422, Sep. 2017.

[11] A. D. Yaghjian, T. B. Hansen, and A. J. Devaney, "Minimum source region for a given far-field pattern," *IEEE Trans. Antennas Propag.*, vol. 45, no. 5, pp. 911–912, May 1997.

[12] R. Zaridze, G. Bit-Babik, K. Tavzarashvili, D. P. Economou, and N. K. Uzunoglu, "Wave field singularity aspects in large-size scatterers and inverse problems," *IEEE Trans. Antennas Propag.*, vol. 50, no. 1, pp. 50–58, Jan. 2002.

[13] A. Capozzoli, C. Curcio, and A. Liseno, "On the optimal field sensing in near-field characterization," *Sensors*, vol. 21, no. 13, p. 4460, Jun. 2021.

[14] E. A. Marengo, A. J. Devaney, and R. W. Ziolkowski, "Inverse source problem and minimum-energy sources," *J. Opt. Soc. Amer. A, Opt. Image Sci.*, vol. 17, no. 1, pp. 34–45, Jan. 2000.

[15] O. Brander and B. DeFacio, "The role of filters and the singular-value decomposition for the inverse born approximation," *Inverse Problems*, vol. 2, no. 4, pp. 375–393, Nov. 1986.

[16] M. Bertero, "Linear inverse and ill-posed problems," in *Advances in Electronics and Electron Physics*, vol. 75, P. W. Hawkes, ed. New York, NY, USA: Academic, 1989, p. 20.

[17] R. Piestun and D. A. B. Miller, "Electromagnetic degrees of freedom of an optical system," *J. Opt. Soc. Amer. A, Opt. Image Sci.*, vol. 17, no. 5, pp. 892–902, 2000.

[18] A. Capozzoli, C. Curcio, A. Liseno, and P. Vinetti, "Field sampling and field reconstruction: A new perspective," *Radio Sci.*, vol. 45, no. 6, Dec. 2010, Art. no. RS6004, doi: 10.1029/2009RS004298.

[19] B. Stupfel and Y. Morel, "Singular value decomposition of the radiation operator—Application to model-order and far-field reduction," *IEEE Trans. Antennas Propag.*, vol. 56, no. 6, pp. 1605–1615, Jun. 2008.

[20] A. Hochman, J. F. Villena, A. G. Polimeridis, L. M. Silveira, J. K. White, and L. Da, "Reduced-order models for electromagnetic scattering problems," *IEEE Trans. Antennas Propag.*, vol. 62, no. 6, pp. 3150–3162, Jun. 2014.

[21] B. Fuchs and A. G. Polimeridis, "Reduced order models for fast antenna characterization," *IEEE Trans. Antennas Propag.*, vol. 67, no. 8, pp. 5673–5677, Aug. 2019.

[22] A. Capozzoli, C. Curcio, and A. Liseno, "Complex waveform generators to effectively test radar systems," *Huawei Antenna Technol. Summit*, Oct. 2019, pp. 23–24.

[23] A. Capozzoli, C. Curcio, and A. Liseno, "An approach for dimensioning equivalent radiators," in *Proc. Antenna Meas. Techn. Assoc. Symp. (AMTA)*, Newport, RI, USA, Nov. 2020, pp. 1–5.

[24] A. Capozzoli, C. Curcio, and A. Liseno, "Scenario modelling in echo generators design," in *Proc. 15th Eur. Conf. Antennas Propag.*, Dusseldorf, Germany, Mar. 2021, pp. 1–4.

[25] A. Capozzoli, C. Curcio, and A. Liseno, "Dimensioning flat, rectangular equivalent radiators," in *Proc. Microw. Medit. Symp. (MMS)*, Pizzo Calabro, Italy, May 2022, pp. 1–4.

[26] M. A. Maisto, R. Solimene, and R. Pierri, "Valid angle criterion and radiation pattern estimation via singular value decomposition for planar scanning," *IET Microw., Antennas Propag.*, vol. 13, no. 13, pp. 2342–2348, Jul. 2019.

[27] K. Atkinson and W. Han, *Spherical Harmonics and Approximations on the Unit Sphere: An Introduction*. Berlin, Germany: Springer-Verlag, 2012.

[28] H. J. Landau and H. O. Pollak, "Prolate spheroidal wave functions, Fourier analysis and uncertainty—III: The dimension of the space of essentially time- and band-limited signals," *Bell Syst. Tech. J.*, vol. 41, no. 4, pp. 1295–1336, Jul. 1962.

[29] B. R. Frieden, "Evaluation, design and extrapolation methods for optical signals, based on use of the prolate functions," in *Progress in Optics*, vol. 9. Amsterdam, The Netherlands: North Holland, 1971, pp. 40–311.

[30] I. B. Risteski and K. G. Trenčevski, "Principal values and principal subspaces of two subspaces of vector spaces with inner product," *Beiträge Algebra Geometrie*, vol. 42, no. 1, pp. 1–12, Jan. 2001.

[31] P. Zhua and A. V. Knyazev, "Principal angles between subspaces and their tangents," Mitsubishi Electr. Res. Lab., Cambridge, MA, USA, Tech. Rep., TR2012-058, Sep. 2012.

Amedeo Capozzoli (Member, IEEE) received the Laurea degree (summa cum laude) in electronic engineering and the Ph.D. degree in electronic engineering and computer science from Università di Napoli Federico II, Naples, Italy.

He is a Full Professor of electromagnetic fields with the Università di Napoli Federico II. His research interests include methods to extract synthetic information on systems of sources or scatterers from field data, adaptive optics in optical astronomy, antenna synthesis and diagnosis, fast numerical methods in electromagnetics, GPU computing in electromagnetics, advanced measurement approaches in electromagnetics, inverse problems, and remote sensing.

Dr. Capozzoli is a Fellow of the *Antenna Measurement Technique Association*. His honors and distinctions has been awarded include the Telecom Italia Prize for the best thesis in Electronic Engineering that was defended at Università di Napoli Federico II, the Barzilai Prize for young scientists in 2002, the Italian Society of Electromagnetism, the Best Technical Paper Award, the Antenna Measurement Technique Association (AMTA) in two consecutive years in 2009 and 2010, the Honorable Mention at the *5th European Conference on Antennas and Propagation* (EuCAP 2011), the Nomination for the Best Paper Award at the *8th European Conference on Antennas and Propagation* (EuCAP 2014) and at the *12th European Conference on Antennas and Propagation* (EuCAP2018). Since 2013, he has been responsible for the *Course on Antenna Synthesis* in the framework of the European School of Antennas (ESoA). In December 2016, he received the 2016 Best Italian EMC Poster Prize at the IEEE EMC Young Professional Paolo Corona Day. He has been Co-Author of papers which received the Mini-Circuits Harvey Kaylie Best Student Paper Award at IEEE-COMCAS in 2021 and the Best Student Paper Award from the *Antenna Measurement Techniques Association* in 2021. He is a Founder and Chair of the Italian AMTA node, the first European node of the *Antenna Measurement Technique Association*. He is also a Chair of the Microwave and Millimeter Wave Lab and of the Numerical Electromagnetics Lab at Università di Napoli Federico II.

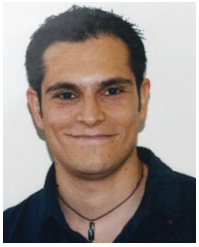

Claudio Curcio (Member, IEEE) received the Laurea degree (summa cum laude) in electronic engineering and the Ph.D. degree in electronic and telecommunication engineering from the Università di Napoli Federico II, Naples, Italy, in 2002 and 2005, respectively.

In 2006 to 2007, he held a Post-Doctoral position at the Università di Napoli Federico II. He is currently Associate Professor with the Università di Napoli Federico II. His main fields of interest are antenna measurements, standard and phaseless effective near-field/far-field transformation techniques, optical beamforming techniques for array antennas, array, and reflectarray synthesis.

Dr. Curcio has been a member of the Applied Computational Electromagnetic Society Since 2012, and since 2018 he is a member of the Institute of Electrical and Electronic Engineering (IEEE). In February 2002, he won the Optimus Award at the SIMAGINE 2002 "Worldwide GSM and Java Card Developer Contest". In the 2009 and 2010, he received the Best Technical Paper Award at the *Antenna Measurement Techniques Association Symposium*. In the 2011 he was ecipient of the Honorable Mention for the Best Antenna Measurement Paper at the *European Conference on Antennas and Propagation* (EUCAP), in 2013 and 2018, he was finalist for the Antenna Measurements Best Paper Award at the EUCAP. In the 2016 he received the IEEE Best Italian EMC Poster Prize from the IEEE EMC Society, Italy Chapter. He has been Co-Author of papers which received the Mini-Circuits Harvey Kaylie Best Student Paper Award at IEEE-COMCAS in 2021 and the Best Student Paper Award from the Antenna Measurement Techniques Association in 2021. Since May 2020, he is member of the IEEE Working Group for the revision of the Standard IEEESTD1720, Recommended Practice for Near-Field Antenna Measurements. He is an Associate Editor for IEEE *Access*.

Angelo Liseno was born in Italy in 1974. He received the Laurea degree (summa cum laude) and the Ph.D. degree in electrical engineering from the Seconda Università di Napoli, Aversa, Italy in 1998 and 2001, respectively.

In 2001 to 2002, he held a Post-Doctoral position at the Seconda Università di Napoli. In 2003 to 2004, he was a Research Scientist with the Institut für Hochfrequenztechnik und Radarsysteme of the Deutsches Zentrum für Luft- und Raumfahrt (DLR), Oberpfaffenhofen, Germany. He is currently an Associate Professor with the Dipartimento di Ingegneria Elettrica e delle Tecnologie dell'Informazione, Università di Napoli Federico II. His main fields of interest are parallel computing techniques for electromagnetics, general purpose GPU computing, complex and phaseless near-field/far-field transformation techniques, antenna synthesis, remote sensing, and inverse scattering, imaging and tomography.

He was awarded the Best Technical Paper Award from the *Antenna Measurement Technique Association* (AMTA) in two consecutive years in 2009 and 2010, the Honorable Mention at the *5th European Conference on Antennas and Propagation* (EuCAP 2011), the Nomination for the Best Paper Award at the *8th European Conference on Antennas and Propagation* (EuCAP 2014) and at the *12th European Conference on Antennas and Propagation* (EuCAP2018). He also received the 2016 Best Italian EMC Poster Prize at the IEEE EMC Young Professional Paolo Corona Day. He has been coauthor of papers which received the Mini-Circuits Harvey Kaylie Best Student Paper Award at IEEE-COMCAS in 2021 and the Best Student Paper Award from the Antenna Measurement Techniques Association in 2021. He is an Associate Editor of IET *Microwaves, Antennas and Propagation, of the International Journal of Antennas and Propagation and Advanced Electromagnetics*.

Open Access funding provided by 'Università degli Studi di Napoli "Federico II"' within the CRUI CARE Agreement